DOI: 10.1021/ma902781e

Macromolecules
ARTICLE

Structure Evolution in Segmented Poly(ester urethane) in Shape-Memory Process

Wei Wang, Ying Jin, Peng Ping, Xuesi Chen, Xiabing Jing, and Zhaohui Su*

State Key Laboratory of Polymer Physics and Chemistry, Changchun Institute of Applied Chemistry, and Graduate School of Chinese Academy of Sciences, Chinese Academy of Sciences, Changchun 130022, P. R. China

Received December 16, 2009; Revised Manuscript Received February 9, 2010

ABSTRACT: A segmented poly(ester urethane) shape-memory polymer with poly(ε-caprolactone) (PCL) soft segment and urethane hard segment was studied by FTIR to investigate the structural evolution in the shape-memory cycle. It was revealed that in the cold drawing programming process, first the amorphous PCL chains start to orient along the drawing direction, and then, the hard segment and the crystalline PCL chains orient upon further extension, accompanied by the weakening of the hydrogen bonds along the drawing direction between the hard segments and stress-induced disaggregation and recrystallization of the crystalline PCL. In the recovery process, the hard segments restore first with the parallel hydrogen bonds strengthening and then the amorphous PCL chains restore the original random orientation, and finally the crystalline PCL chains lose their alignment to a less-oriented state.

Introduction

In recent years, shape-memory polymers (SMPs) have attracted a great deal of attention because they are able to remember and recover their permanent shape after deformation under certain stimulus such as heat or light[1−9] and thus may find application in smart fabrics,[10] intelligent medical devices,[11] minimally invasive surgery,[12,13] and other fields. In general, an SMP consists of two components: the net points determine the permanent shape and can be achieved by either physical interactions or chemical bonds, imparting a level of rigidity, dimensional stability, and thermal resistance, and the switching segments are associated with the temporary shape and can be either amorphous or crystalline. The shape-memory effect is largely dependent on the morphology and the degree of microphase separation of the copolymer, which in turn are determined by the molecular characteristics such as the molecular weight and the composition of the two segments.[4−6,14] The shape-memory process of the heat-stimulus SMPs is called programming. In the traditional thermal programming,[4,6] the sample is first heated to above the transition temperature (T_{trans}), which is either the glass-transition temperature or the melting temperature of the switching segments, and then deformed and cooled to freeze its temporary shape, and later on, when the environment temperature rises to above T_{trans}, the deformed SMP restores its permanent shape. Another processing method is called cold drawing programming, which is illustrated in Scheme 1. This programming is done at lower temperatures (below T_{trans}) and has the benefit of more convenient processing, lower recovery temperatures, and largely enhanced recovery stress.[7,15]

As an important class of thermoplastic SMP, segmented polyurethane has two kinds of segments, with the hard segments as the net points and the soft segments as the switching segments.[3−6] The hard segments are based on diisocynates and diols, and the soft segments are either polyethers or polyesters. By the introduction of biodegradable polyesters such as poly(L-lactic acid) and poly(ε-caprolactone) (PCL) into the SMP,[7,12,16] the material can exhibit both biodegradability and shape-recoverability and is expected to find extensive application in medical devices and implants. A great deal of studies have focused on the synthesis, medical applications, and thermal properties of segmental polyurethanes; however, reports on the structural characters of the phase transitions and the associated shape-memory effect are rare.[17−19]

For segmented copolymers in general, their morphological features during deformation have been studied,[20−23] and various experimental methods such as small-angle X-ray scattering (SAXS),[24−26] wide-angle X-ray diffraction (WAXD),[26,27] dynamic mechanical thermal analysis (DMTA),[28] and atomic force microscopy (AFM)[29,30] have been employed to elucidate the morphological and structural changes and chain orientation. Whereas these methods mainly assess the structure of the crystalline domains, molecular spectroscopy, in particular, FTIR, can provide quantitative structural information of both crystalline and amorphous domains based on the infrared dichroism of the specific bands during the deformation process.[20−24,27,31,32] In the present study, FTIR was employed to monitor the shape-memory process of a segmented poly(ester urethane) (PEU) during the cold drawing programming in an attempt to reveal the shape-memory mechanism of the cold drawing programming of SMPs.

Experimental Section

Sample Preparation. A segmented PEU SMP with PCL as the soft segment and 2,4-toluene diisocyanate (TDI)−ethylene glycol (EG) as the hard segment, shown in Scheme 2, was used in this study. The molecular weight of the soft segment was 5000, and the composition was PCL/TDI/EG 1:5:4. The melting temperature of the soft segment was 55 °C, and the hard segment was amorphous. Details of the PEU sample synthesis and thermomechanical and shape-memory properties were previously reported.[7] We prepared thin films of $< 15\ \mu$m thickness by casting a PEU chloroform solution on glass slides, which maintained under vacuum at 40 °C for 24 h to remove the chloroform. Then, the films were peeled off from the glass slides in water and maintained under vacuum for 2 h. The films were cut into stripes of 20 × 10 mm size for mechanical

*To whom correspondence should be addressed. Tel: (86)431-85262854. Fax: (86)431-85262126. E-mail: zhsu@ciac.jl.cn.

 Published on Web 02/23/2010

Scheme 1. Schematic Illustration of the Cold Drawing Programming of SMPs

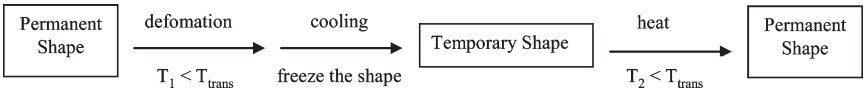

Scheme 2. Chemical Structure of the PEU

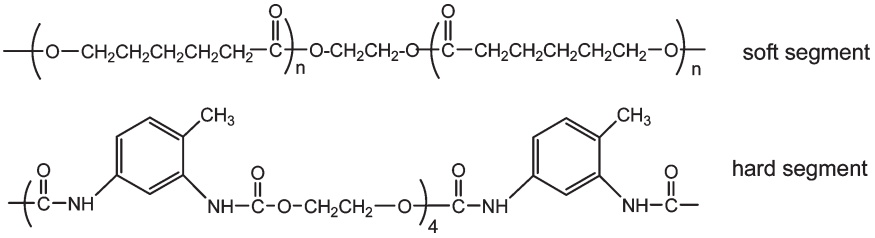

measurements, and the initial length between the clamps of the stretching device was 8 mm.

Instrumentation. The cold drawing and recovery of the PEU films was accomplished with a homemade stretching device mounted in the sample chamber of the FTIR. The cold drawing was performed at 25 °C and the recovery at 36 °C. The specimen was allowed to relax for 1 min at each strain before the spectrum was collected. FT-IR spectra were recorded on a Bruker Vertex-70 spectrometer equipped with a DTGS detector with 16 scans coadded at a resolution of 2 cm^{-1}. The polarized spectra of the PEU films during the cold drawing and recovery processes were measured with the radiation polarized parallel and perpendicular to the drawing direction, respectively. Differential scanning calorimetry (DSC) was performed on a TA Q-100 calorimeter at a 10 °C/min scan rate under a nitrogen atmosphere.

Data Processing. The orientation of chain segments is characterized by the orientation function defined as[33,34]

$$f = \frac{3 < \cos^2 \theta > -1}{2} \quad (1)$$

where θ is the angle between the chain axis and the drawing direction, and a perfectly parallel, perfectly perpendicular, and random orientation corresponds to $f = 1$, -0.5, and 0, respectively. The infrared dichroism for determination of the orientation function follows the formula[34]

$$f = \frac{(R_0 + 2)(R - 1)}{(R_0 - 1)(R + 2)} \quad (2)$$

where $R_0 = 2ctg^2\alpha$, where α is the angle between the transition moment and the chain axis, and R is the infrared dichroic ratio with $R = A_{\parallel}/A_{\perp}$, $A_{\parallel}$, and $A_{\perp}$ being the absorbance of the parallel and perpendicular spectra, respectively. In this work, peak areas were chosen over peak heights for all the quantitative analyses because peak positions may shift under extension, which is also discussed later in this article.

Figure 1 shows the polarized spectra of the PEU at 150% strain. The 1535 cm^{-1} band, assigned to N−H bending and C−N stretching, was used to calculate the orientation function of the hard segment because the amides only exist in the hard segment and the band is well separated from the infrared bands of the soft segments. This band has a parallel dichroism, and taking $\alpha = 0°$,[32] formula 2 leads to

$$f_H = \frac{R(1535) - 1}{R(1535) + 2} \quad (3)$$

The 1295 cm^{-1} band, assigned to C−C and C−O stretching, was used to calculate the orientation function of the crystalline PCL soft segments because it only exists in the PCL crystalline phase. This band has a parallel dichroism, and taking

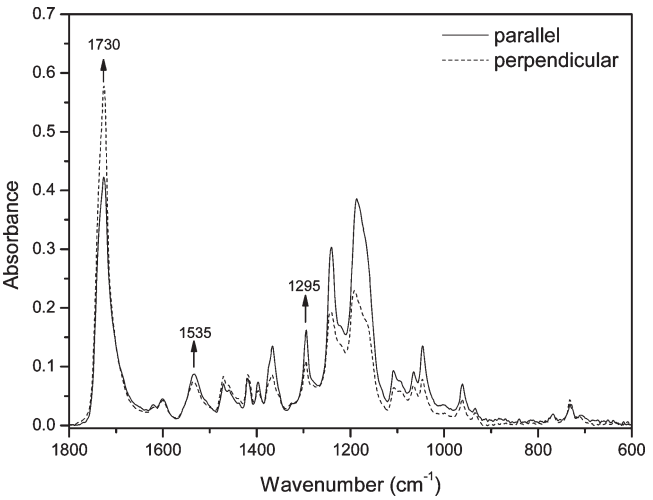

Figure 1. Polarized infrared spectra of the PEU film stretched to 150%, with the drawing direction as the reference direction.

$\alpha = 0°$,[35,36] formula 2 leads to

$$f_{S,cr} = \frac{R(1295) - 1}{R(1295) + 2} \quad (4)$$

The around 1730 cm^{-1} arises from the carbonyl groups of the crystalline PCL (1724 cm^{-1}), the amorphous PCL (1736 cm^{-1}), and the urethane (1710 and 1696 cm^{-1}) in the hard segment. The PCL carbonyl band (sum of the bands at 1724 and 1736 cm^{-1}) was used to calculate the average orientation function of PCL in both phases, and taking $\alpha = 78°$,[36] formula 2 leads to

$$f_{S,av} = -2.3\frac{R(COO) - 1}{R(COO) + 2} \quad (5)$$

and the orientation function of the amorphous PCL can be deduced from the following formula[36]

$$f_{S,am} = \frac{f_{S,av} - X_c f_{S,cr}}{1 - X_c} \quad (6)$$

where X_c is the crystallinity of the PCL soft segment, and it can be obtained using the following formula[37]

$$X_c = \frac{A_0(1724)}{A_0(1724) + 1.46A_0(1736)} \quad (7)$$

where $A_0(1724)$ and $A_0(1736)$ are the band areas of the crystalline and amorphous PCL, respectively, and can be obtained via

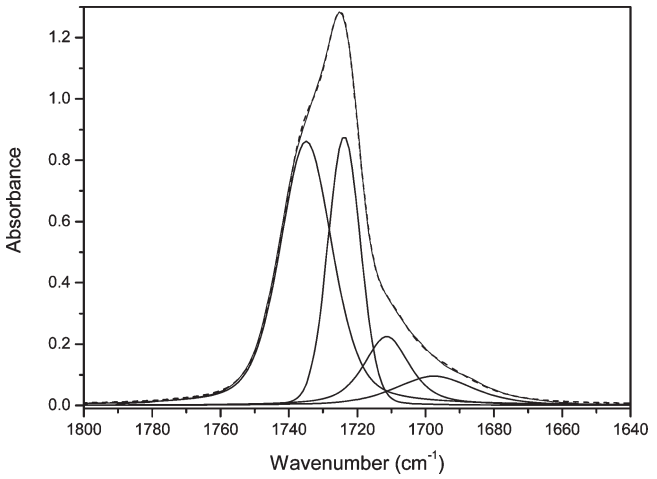

Figure 2. Curve fitting of the carbonyl band in the 1800−1640 cm^{-1} region.

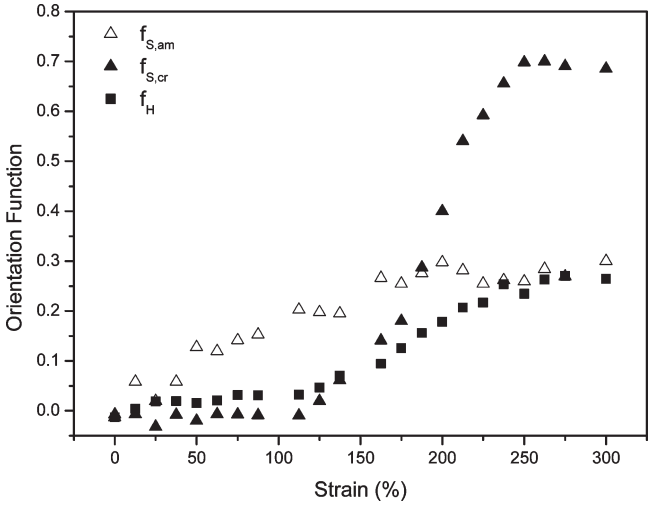

Figure 3. Orientation function versus strain for the PEU stretched at 25 °C (△, amorphous PCL; ▲, crystalline PCL; ■, hard segment).

curve fitting.[37] The curve fitting of the carbonyl band was done using the local-least-squares routine provided in the OPUS software package. The adopted procedure used four parameters, peak position, intensity, band width, and shape, which were allowed to vary upon iteration, and the "best" fitting was obtained as the root-mean-square deviation was minimized. The curve fitting results are shown in Figure 2. The crystallinity of the PCL soft segment thus obtained by IR was ∼30%, in agreement with that measured by DSC (30.5%), which validates the curve fitting routine. The hard segment content in the PEU was 18.3%; therefore, the crystalline and the amorphous PCL was 25 and 55% of the total weight, respectively.

Results and Discussion

Drawing Process. Figure 3 shows the orientation functions of the amorphous and crystalline PCL and the urethane hard segment plotted versus the strain at 25 °C. Whereas for homo PCL, the crystalline orientation function increases rapidly upon stretching,[36] the PCL soft segments in the copolymer behave differently. There are three distinct stages in the drawing process. In the first stage (up to about 100% strain), the orientation function of the amorphous PCL gradually increases upon extension, whereas that of the crystalline PCL and the hard segment exhibits very small negative and positive values, respectively, indicating that the amorphous PCL segments connecting the crystalline PCL and the urethane hard domains start to extend and orient along the drawing direction, which relaxes much of the stress, and the latter two phases have not experienced much of the stretch. The slightly negative orientation function of the crystalline PCL at small extensions indicates a weak perpendicular orientation, which may be attributed to the interlamella separation, which has been reported for isotactic polypropylene[38] and polyurethane.[31] In the second stage (∼100 to 250% strain), the orientation function of the amorphous PCL continues to increase, and reaches its maximum of ∼0.25, whereas the orientation function of the crystalline PCL starts to increase steeply, and a moderate increase in orientation is observed for the hard segment. In this stage, the amorphous PCL segments are further stretched and orient more parallel to the stretch direction, approaching its maximum, and pass the stress on to the crystalline PCL and the urethane hard domains, the "hard" blocks serving as the net points, which now start to orient along the stretch direction. In the third stage (above 250%), the orientation functions of the crystalline PCL and the hard segment level off at their respective maximum.

Figure 4a shows under extension the frequency shift of the CNH vibration characteristic of the urethane hard segment at ∼1535 cm^{-1}. Whereas the perpendicular component of the peak remains almost constant, for the parallel component, the frequency first decreases slightly at small extensions (below 100% strain) and then shifts more steeply upon further stretching and reaches a minimum at ∼250% strain. At 300% strain, the parallel component exhibits a negative frequency shift of ∼4 cm^{-1}. The parallel spectra showing the shift are included in the Supporting Information. The shift of the N−H bending, the major component of the 1535 cm^{-1} band, to lower frequency is attributed to the weakening of the hydrogen bonds upon extension.[39] This trend is similar to that of the orientation function of the hard segment, indicating that the orientation of the hard segment is accompanied by the weakening of the hydrogen bonds upon extension.

Similar frequency shift was observed for the C−C and C−O stretching band located at ∼1295 cm^{-1}, which is characteristic of the crystalline PCL, as shown in Figure 4b. The perpendicular component is almost constant over the entire stretching process, but the parallel component shows a negative frequency shift of ∼2 cm^{-1} upon extension to 300% strain, and the trend is similar to the variation of the orientation function of the crystalline PCL in the same process. The frequency shift is from the crystalline regions where the C−C and C−O bonds are parallel to the *c* axis of the crystal, indicating that the PCL crystals are experiencing high tensile stress. It has been well established that this kind of tensile stress would induce rapid disaggregation and recrystallization in semicrystalline polymers such as PCL and HDPE, and the overall degree of crystallinity would remain the same in this process.[40,41] Figure 4c plots the PCL crystallinity determined by FTIR via eq 7 in the drawing process, which shows that the crystallinity is essentially constant from 0 to 300% extension. In a separate experiment, films as cast and stretched to various extensions were analyzed by DSC (Figure 4d), and the PCL degrees of crystallinity obtained for these samples were 30.5, 31.7, 32.2, 30.3, 30.9, and 31.4%, respectively, indicating that the PCL crystallinity is independent of the strain, and the average was 31.2%, both in good agreement with the IR results. It is also interesting to see in Figure 4d that the shapes of the melting peaks are different for these samples, and in general, the melting peak for the stretched films shifts to lower temperatures compared with the unstretched sample,

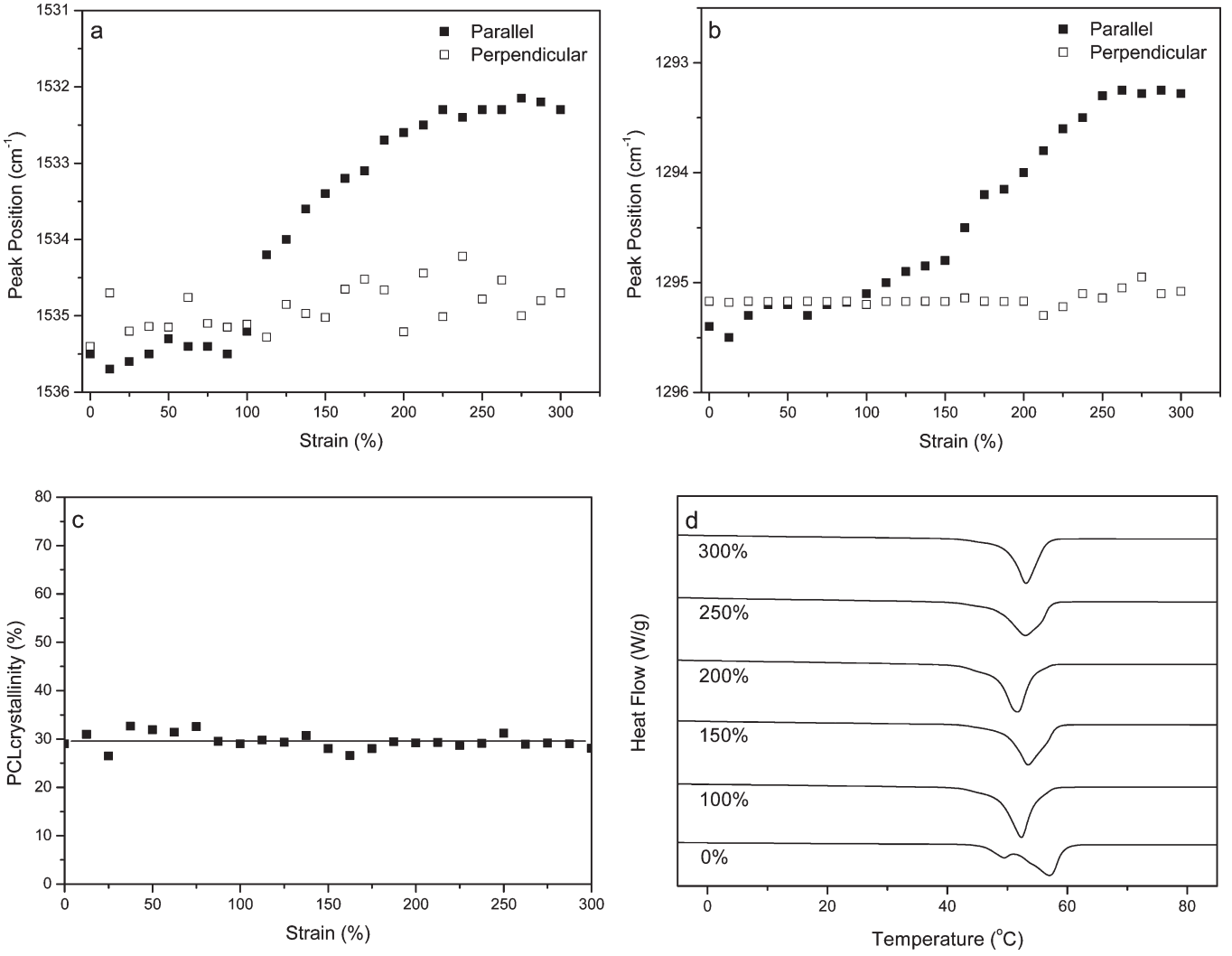

Figure 4. Plots of peak position of the (a) 1535 and (b) 1295 cm^{-1} bands and (c) the PCL crystallinity versus strain during the cold drawing process and (d) the DSC heating traces of the film at various strains.

suggesting that the size or perfection of the crystals have changed when the film is under extension, an evidence of crystal disaggregation and recrystallization.[40,41] These results suggest that at high extensions, the PCL soft segments undergo rapid disaggregation and recrystallization, leading to more smaller crystals, which together with the now oriented urethane hard domains fixes the material in the deformed shape.

Recovery Process. Because of the fast recovery rate at 40 °C (the typical recovery temperature for this SMP[7]), for the convenience of the experiment, we chose to study the recovery process at 36 °C. Figure 5 plots the orientation functions of the amorphous and crystalline PCL and the urethane hard segment versus the strain of the PEU during the recovery process. It can be seen that first the orientation function of the hard segment starts to decrease at 165% extension and goes down to 0 at ~140% strain; then, the amorphous PCL starts to lose its preferred orientation at ~150% strain and becomes randomly oriented when the PEU recovers to ~130% strain. The crystalline PCL retains its orientation at small recovery, which then decrease fairly quickly when the strain reduces from ~140 to 100% and then slowly goes down when the sample further recovers. These results indicate that in the recovery process, the hard segments restore first, maybe because of the strengthening of the hydrogen bonds discussed below, recovering the randomly

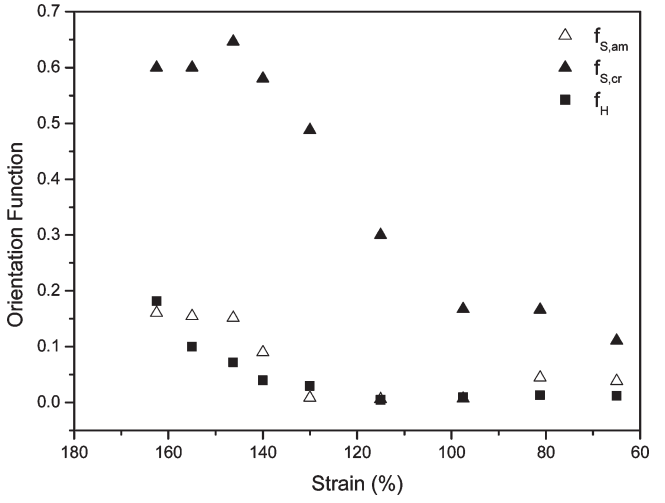

Figure 5. Orientation function versus strain recovery for the PEU at 36 °C (△, amorphous PCL; ▲, crystalline PCL; ■, hard segment).

oriented state and serving as the physical cross-links, and then the stretched and oriented amorphous PCL chains between the "hard" domains retract and lose their preferred orientation. With the retraction of the amorphous domains,

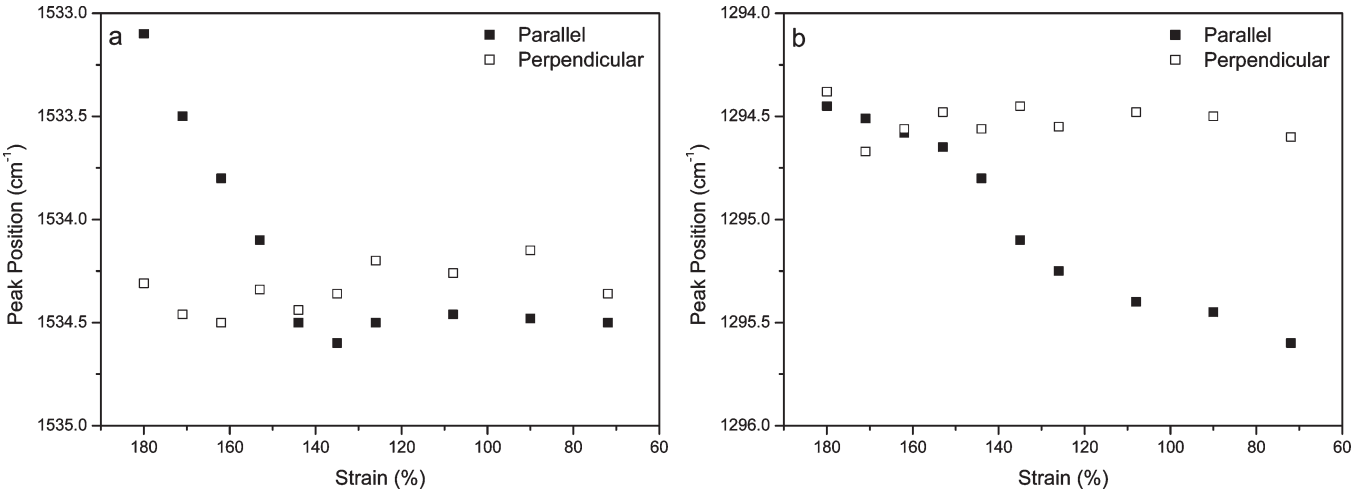

Figure 6. Plots of peak position versus strain during the recovery process of (a) the 1535 band and (b) the 1295 cm^{-1} band.

Scheme 3. Schematic Illustration of the Structural Evolution of the PEU SMP during the Cold Drawing and the Recovery Processes

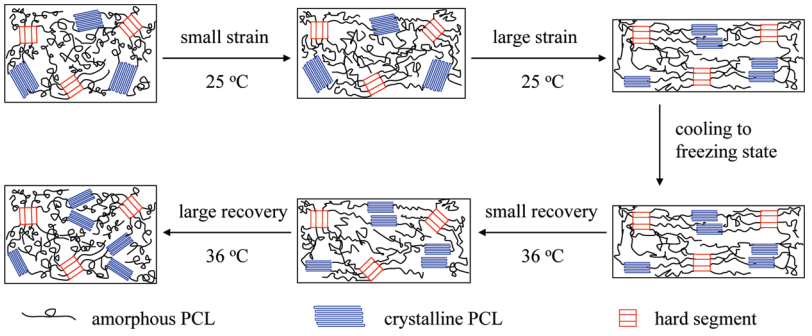

the crystalline PCL chains lose their alignment and partially recover to the original state with some residual orientation, which probably is due to irreversible deformation of the lamellae in the drawing process.

Figure 6a shows the frequency shift of the 1535 cm^{-1} band, which is primarily from the N−H bending. The parallel component shows a positive frequency shift of ∼2 cm^{-1}, and the perpendicular component is almost constant. The positive frequency shift is an indication of strengthening of the hydrogen bonds.[39] The frequency shifts rapidly first and reaches a maximum at ∼140% strain and then remains constant upon further recovery. This trend is similar to that of the orientation function of the hard segments, revealing that during the recovery process, the hard segments form stronger hydrogen bonds while losing the orientation, the opposite of what we observed in the stretching process.

The frequency shift of the C−C and C−O stretching band located at ∼1295 cm^{-1} is shown in Figure 6b. The parallel component exhibits a positive frequency shift of ∼1 cm^{-1}, and the perpendicular component does not change, which is indicative of the release of the stress applied to the PCL crystals. This allows the crystals to rotate and adopt a more random orientation. The trend of the frequency shift is similar to that of the orientation function of the crystalline PCL during the recovery process.

Summary

On the basis of the experimental results discussed above, we can now summarize the evolution of the microstructure of the segmented PEU SMP in the cold drawing and the recovery processes. This is schematically illustrated in Scheme 3. In the cold drawing programming, the amorphous PCL chains orient first at small extensions, whereas the hard segments and the crystalline PCL largely maintain their original state. When stretched further, the hard segments and the crystalline PCL chains start to align along the stretching direction and quickly reach a high degree of orientation; the hydrogen bonds between the urethane units along the stretching direction are weakened, and the PCL undergoes stress-induced disaggregation and recrystallization while maintaining its overall crystallinity. The SMP now adopts its temporary shape fixed by the oriented hard domains and the newly formed PCL crystals. When the temperature is increased, the SMP starts to recover to its permanent shape. The hard segments start to restore first at small recovery, and the hydrogen bonds along the extension direction between the urethane units become stronger; then, the amorphous PCL segments connecting the hard and the crystalline domains restore to the original random orientation state, and finally the crystalline PCL chains lose their alignment via rotation to a less-oriented state. Eventually, the SMP is back to its original shape and is ready for the next cycle of the shape-memory process. This detailed understanding of the structure evolution of SMPs at the molecular level associated with the shape-memory effect may help the design of better SMPs for potential applications in various fields.

Acknowledgment. We thank Prof. Yongfeng Men for helpful discussion. The financial support from the National Natural Science Foundation of China (20774097) is acknowledged. Z.S. thanks the NSFC Fund for Creative Research Groups (50921062) for support.

Supporting Information Available: Parallel spectra of the SMP film showing the frequency shifts under stretch for bands

at ~1295 and ~1535 cm^{-1}. This material is available free of charge via the Internet at http://pubs.acs.org.

References and Notes

(1) Ratna, D.; Karger-Kocsis, J. *J. Mater. Sci.* **2008**, *43*, 254–269.
(2) Lendlein, A.; Jiang, H. Y.; Junger, O.; Langer, R. *Nature* **2005**, *434*, 879–882.
(3) Lee, B. S.; Chun, B. C.; Chung, Y. C.; Sul, K. I.; Cho, J. W. *Macromolecules* **2001**, *34*, 6431–6437.
(4) Lendlein, A.; Kelch, S. *Angew. Chem., Int. Ed.* **2002**, *41*, 2034–2057.
(5) Behl, M.; Lendlein, A. *Mater. Today* **2007**, *10*, 20–28.
(6) Liu, C.; Qin, H.; Mather, P. T. *J. Mater. Chem.* **2007**, *17*, 1543–1558.
(7) Ping, P.; Wang, W. S.; Chen, X. S.; Jing, X. B. *Biomacromolecules* **2005**, *6*, 587–592.
(8) Beloshenko, V. A.; Varyukhin, V. N.; Voznyak, Y. V. *Russ. Chem. Rev.* **2005**, *74*, 265–283.
(9) Lee, K. M.; Knight, P. T.; Chung, T.; Mather, P. T. *Macromolecules* **2008**, *41*, 4730–4738.
(10) Ji, F. L.; Zhu, Y.; Hu, J. L.; Liu, Y.; Yeung, L. Y.; Ye, G. D. *Smart Mater. Struct.* **2006**, *15*, 1547–1554.
(11) Wache, H. M.; Tartakowska, D. J.; Hentrich, A.; Wagner, M. H. *J. Mater. Sci.: Mater. Med.* **2003**, *14*, 109–112.
(12) Lendlein, A.; Langer, R. *Science* **2002**, *296*, 1673–1676.
(13) Metcalfe, A.; Desfaits, A. C.; Salazkin, I.; Yahia, L.; Sokolowski, W. M.; Raymond, J. *Biomaterials* **2003**, *24*, 491–497.
(14) Ji, F. L.; Hu, J. L.; Li, T. C.; Wong, Y. W. *Polymer* **2007**, *48*, 5133–5145.
(15) Ping, P. Ph.D. Thesis, Changchun Institute of Applied Chemistry, Chinese Academy of Sciences: Changchun, China, **2005**.
(16) Wang, W. S.; Ping, P.; Chen, X. S.; Jing, X. B. *Eur. Polym. J.* **2006**, *42*, 1240–1249.
(17) Wang, W.; Wang, W.; Chen, X.; Jing, X.; Su, Z. *J. Polym. Sci., Part B: Polym. Phys.* **2009**, *47*, 685–695.
(18) Wang, M. T.; Zhang, L. D. *J. Polym. Sci., Part B: Polym. Phys.* **1999**, *37*, 101–112.
(19) Diani, J.; Gall, K. *Smart Mater. Struct.* **2007**, *16*, 1575–1583.
(20) Lin, S. B.; Hwang, K. S.; Tsay, S. Y.; Cooper, S. L. *Colloid Polym. Sci.* **1985**, *263*, 128–140.
(21) Lee, H. S.; Lee, N. W.; Paik, K. H.; Ihmt, D. W. *Macromolecules* **1994**, *27*, 4364–4370.
(22) Chuah, H. H. *Macromolecules* **2001**, *34*, 6985–6993.
(23) Duan, Y. X.; Rettler, E.; Schneider, K.; Schlegel, R.; Thunga, M.; Weidisch, R.; Siesler, H. W.; Stamm, M.; Mays, J. W.; Hadjichristidis, N. *Macromolecules* **2008**, *41*, 4565–4568.
(24) Lee, H. S.; Yoo, S. R.; Seo, S. W. *J. Polym. Sci., Part B: Polym. Phys.* **1999**, *37*, 3233–3245.
(25) Tang, Y. J.; Jiang, Z. Y.; Men, Y. F.; An, L. J.; Enderle, H. F.; Lilge, D.; Roth, S. V.; Gehrke, R.; Rieger, J. *Polymer* **2007**, *48*, 5125–5132.
(26) Zhang, Y.; Prud′homme, R. E. *Macromol. Rapid Commun.* **2006**, *27*, 1565–1571.
(27) Yeh, F.; Hsiao, B. S.; Sauer, B. B.; Michel, S.; Siesler, H. W. *Macromolecules* **2003**, *36*, 1940–1954.
(28) Madbouly, S. A.; Ougizawa, T. *J. Macromol. Sci., Phys.* **2003**, *42*, 269–281.
(29) Thomas, C.; Ferreiro, V.; Coulon, G.; Seguela, R. *Polymer* **2007**, *48*, 6041–6048.
(30) Nie, H.-Y.; Walzak, M. J.; McIntyre, N. S. *Polymer* **2000**, *41*, 2213–2218.
(31) Dai, X. H.; Xu, J.; Guo, X. L.; Lu, Y. L.; Shen, D. Y.; Zhao, N.; Luo, X. D.; Zhang, X. L. *Macromolecules* **2004**, *37*, 5615–5623.
(32) Graff, D. K.; Wang, H. C.; Palmer, R. A.; Schoonover, J. R. *Macromolecules* **1999**, *32*, 7147–7155.
(33) Siesler, H. W. *Adv. Polym. Sci.* **1984**, *65*, 1–77.
(34) Koenig, J. L. *Spectroscopy of Polymers*, 2nd ed.; Elsevier: New York, 1999.
(35) Zhao, Y.; Keroack, D.; Prud′homme, R. *Macromolecules* **1999**, *32*, 1218–1225.
(36) Keroack, D.; Zhao, Y.; Prud′homme, R. E. *Polymer* **1998**, *40*, 243–251.
(37) He, Y.; Inoue, Y. *Polym. Int.* **2000**, *49*, 623–626.
(38) Huy, T. A.; Adhikari, R.; Lupke, T.; Henning, S.; Michler, G. H. *J. Polym. Sci., Part B: Polym. Phys.* **2004**, *42*, 4478–4488.
(39) Loo, L. S.; Gleason, K. K. *Macromolecules* **2003**, *36*, 6114–6126.
(40) Men, Y. F.; Rieger, J.; Strobl, G. *Phys. Rev. Lett.* **2003**, *91*, 095502.
(41) Jiang, Z. Y.; Tang, Y. J.; Men, Y. F.; Enderle, H. F.; Lilge, D.; Roth, S. V.; Gehrke, R.; Rieger, J. *Macromolecues* **2007**, *40*, 7263–7269.